^{4}He, ^{10}Be, ^{14}C, and ^{16}O light-fragment-accompanied cold ternary fission of the ^{250}Cm isotope in an equatorial three-cluster model

M. R. Pahlavani,* O. N. Ghodsi,† and M. Zadehrafi‡
Department of Nuclear Physics, Faculty of Basic Science, University of Mazandaran, P.O. Box 47415-416, Babolsar, Iran
(Received 18 September 2017; revised manuscript received 17 October 2017; published 29 November 2017)

The cold ternary fission of ^{250}Cm accompanied with ^{4}He, ^{10}Be, ^{14}C, and ^{16}O light charged particles in the equatorial three-cluster model configuration is studied. Driving potential and fission yield for each accompanied light charged particles for individual fragmentation are calculated. The obtained results reveal that even-mass-number components are more favored than odd-mass-number components. Furthermore, upon increasing the mass of light fixed fragment in ternary fission, the probability of crossing over the potential barrier (driving potential) is decreased considerably due to the height of the potential barrier. The comparison between relative yields for a variety of fragmentation in each group indicates that the presence of doubly or near doubly magic closed-shell fragments are more favored in the cold ternary fission of the ^{250}Cm superheavy isotope.

DOI: 10.1103/PhysRevC.96.054612

I. INTRODUCTION

With the advent of fission and its application to produce nuclear energy in the late 1940s, most attempts focused logically on products of binary fission. Ternary fission was recognized as a curious source of energetic alpha particles. This rare type of fission was discovered by Chinese scientists in cooperation with French researchers [1–5]. Tritium gas emitted in thermal-neutron-induced ternary fission of the ^{249}Cf isotope was observed for the first time in the Laue–Langevin Institute located in Grenoble (France) [6]. Also, tritium as a ternary fission product was discovered by monitoring fission fuel wastes [7,8]. The spontaneous breakup of a superheavy nucleus into three fission fragments is referred to as cold ternary fission and has been considered as a very rare process compared with binary fission. Usually, one of the ternary fission fragments is much lighter than the other two main fragments and hence the ternary fission is often referred to as a light-charged-particle-accompanied (LCP-accompanied) process. In most cases of ternary fission, the light fixed fragment is emitted in a direction perpendicular to the other two fission fragments due to the formation of the LCP in the neck region. Hence, LCP is accelerated due to the Coulomb repulsion of both heavy fragments after emission in the perpendicular direction relative to the main fragments. Such a process is called LCP-accompanied equatorial ternary fission. However, in true ternary fission in which the parent nucleus splits into three fragments of not very different masses, all fragments escape along the same line, which is called collinear ternary fission. True ternary fission mostly occurs in heavy and superheavy nuclei with large values of the fissility parameter, $Z^2/A > 31$ [9]. Also, the energy released in true ternary fission is much larger than that in equatorial LCP-accompanied ternary fission. In spite of huge attempts, the theoretical aspects of this process are not well understood. The probability of LCP-accompanied ternary fission decreases sharply upon increasing the mass number of the accompanying fixed third particle. The first experimental evidence for LCP-accompanied ternary fission was reported by Alverez *et al.* [10]. Because of its importance in competition with binary fission of heavy and superheavy isotopes, this rare process has been studied extensively both theoretically and experimentally [11–23]. A coplanar three-cluster approach was developed to study the cold α particle accompanied ternary fission of ^{252}Cf by using a double folding potential [18]. Rosen and Hudson [24] have shown experimentally that the probability of true ternary fission is much lower than that of binary fission (approximately 6.7 ± 3 per 10^6 binary fission in the ^{235}U isotope). Poenaru *et al.* [25–27] presented a simple theoretical method to study ternary fission. All possible ternary fragmentation of ^{252}Cf isotope have been investigated [28,29] by using three-cluster model (TCM) [30]. Gupta and his colleagues used the TCM to study the decay modes of different isotopes via exotic cluster emissions [31,32]. The effect of deformation and orientation on the ternary fragmentation potential of ^{4}He- and ^{10}Be-accompanied fission of ^{252}Cf has been studied as well [33]. This approach has been used extensively to study the various aspects of ternary fission for different isotopes of californium, plutonium, and curium [9,34–39]. The liquid drop formalism via the Yukawa-plus-exponential nuclear potential along with nuclear shape parametrization are applied to obtain the ternary-to-binary ratio in collinear geometry for the ^{252}Cf isotope [40]. Recently, various isotopes of helium, lithium, beryllium, boron, and carbon (LCPs) were observed in the spontaneous ternary fission of ^{252}Cf [41,42].

In the present investigation, we attempt to apply the TCM to study the ternary fission of the ^{250}Cm isotope accompanied by ^{4}He, ^{10}Be, ^{14}C, and ^{16}O light charged particles as the fixed third fragment. In Sec. II, we present the theoretical aspects of the model. The driving potential and LCP-accompanied probability for each individual fragmentation are calculated by using the equatorial TCM for separate accompanied fixed third fragments in Sec. II. The results obtained are discussed in Sec. III. Finally, a brief summary of the present study along with the concluding remarks are provided in Sec. IV.

*m.pahlavani@umz.ac.ir
†o.nghodsi@umz.ac.ir
‡m.zadehrafi@stu.umz.ac.ir

II. METHODOLOGY

As is well known, each reaction occurs spontaneously only if the Q value of the reaction becomes positive energetically. The Q value of cold ternary fission must satisfy the following condition:

$$Q = M - \sum_{i=1}^{3} m_i > 0, \tag{1}$$

where M is the mass excess of the parent nucleus undergoing ternary fission and m_i are the mass excesses of the three fragments expressed in energy units. Note that Q is the released energy in the reaction and can be defined by $Q = E_1 + E_2 + E_3$ with E_i $(i = 1,2,3)$ being the kinetic energy carried by the three individual fragments.

For a heavy unstable parent nucleus that undergoes cold ternary fission, the interacting potential between the three nascent fragments is equal to sum of the total Coulomb and nuclear potential,

$$V = \sum_{i=1}^{3} \sum_{j>i}^{3} (V_{Cij} + V_{Pij}), \tag{2}$$

where V_{Pij} and V_{Cij} are nuclear and Coulomb potential between each pair of fragments, respectively. The proximity type of potential is considered for the nuclear interaction of fragment pairs. The Coulomb potential V_{Cij} is related to the repulsion Coulomb force between each pair of fragments and is defined as

$$V_{Cij} = \frac{Z_i Z_j e^2}{R_{ij}}, \tag{3}$$

where Z_i and Z_j are the atomic numbers and R_{ij} is the center-to-center distance between two fragments i and j, respectively. R_x is the net radius of each fragment ($x = 1,2,3$ stands for the three fragments), which is evaluated by using the following semi-empirical formula in terms of fragments mass number A_x:

$$R_x = 1.28A_x^{1/3} - 0.76 + 0.8A_x^{-1/3}. \tag{4}$$

The nuclear proximity potential V_{Pij} is defined as [36]

$$V_{Pij}(s) = 4\pi b\gamma \overline{R}\Phi\left(\frac{s}{b}\right). \tag{5}$$

Here, b is the nuclear surface diffuseness parameter, which is varied in the interval $[0.5,1]$. $b = 0.87$ fm is considered here.

The coefficient of nuclear surface tension, γ, is defined through the Lysekil mass formula [43],

$$\gamma = 0.9517[1 - 1.7826(N - Z)^2/A^2]\ \text{MeV/fm}^2, \tag{6}$$

where N, Z, and A are the neutron, proton, and mass number of the parent nucleus, respectively.

$\overline{R}$ is the mean curvature radius, which is defined by

$$\overline{R} = \frac{R_i R_j}{R_i + R_j}. \tag{7}$$

Finally, $\Phi(\xi) = \Phi(\frac{s}{b})$ is the universal proximity potential function, which is a function of the distance between two interacting fragments [44],

$$\Phi(\xi) = \begin{cases} -\frac{1}{2}(\xi - 2.54)^2 - 0.0852(\xi - 2.54)^3 & \text{for} \quad \xi < 1.2511 \\ -3.437\exp(-\xi/0.75) & \text{for} \quad \xi \geqslant 1.2511, \end{cases} \tag{8}$$

where $\xi = s/b$ is a straight function of distance between fragments and $s_{ij}(= R_{ij} - R_i - R_j)$ is the distance between near surfaces of the fragments. In the equatorial configuration, it is usual to consider $s = s_{12} = s_{13} = s_{23}$. It means the three ternary fission products are separated from each other symmetrically with the same speed. In reality, the light fragment goes away faster than the two heavier ones. For simplicity, as a reliable approximation, one may consider equivalent speeds for three fragments [28,29,33]. Also, $s = 0$, $s < 0$, and $s > 0$ correspond to the "touching configuration," "overlap region," and "separated fragments" structure, respectively.

Based on the TCM, the relative yields of all charge-minimized fragmentation channels are calculated as the ratio between the penetration probability of a given fragment over the sum of penetration probabilities of all possible fragmentation:

$$Y(A_i,Z_i) = \frac{P(A_i,Z_i)}{\sum P(A_i,Z_i)}. \tag{9}$$

Here, $P(A_i,Z_i)$ is the probability in which fragment i crosses the three-body potential barrier. The penetration probability is obtained by using the one-dimensional Wentzel-Kramers-Brillouin (WKB) approximation,

$$P = \exp\left\{-\frac{2}{\hbar}\int_{s_1}^{s_2}\sqrt{2\mu(V - Q)}ds\right\}, \tag{10}$$

where V is interaction potential given by Eq. (2) and Q is the energy released in fission, which is defined by Eq. (1).

The first turning point $s_1 = 0$ represents the touching-fragments configuration and the second turning point s_2 satisfies the $V(s_2) = Q$ condition.

The reduced mass of the three fragments is defined as

$$\mu = m\left(\frac{A_1A_2A_3}{A_1A_2 + A_1A_3 + A_2A_3}\right), \tag{11}$$

where m is the average mass of the nucleon and A_1, A_2, and A_3 are the mass numbers of the three fission products.

III. RESULTS AND DISCUSSIONS

The structure of the minima in the so-called driving potential is studied based on the concept of a cold reaction valley. The difference between the interaction potential V and

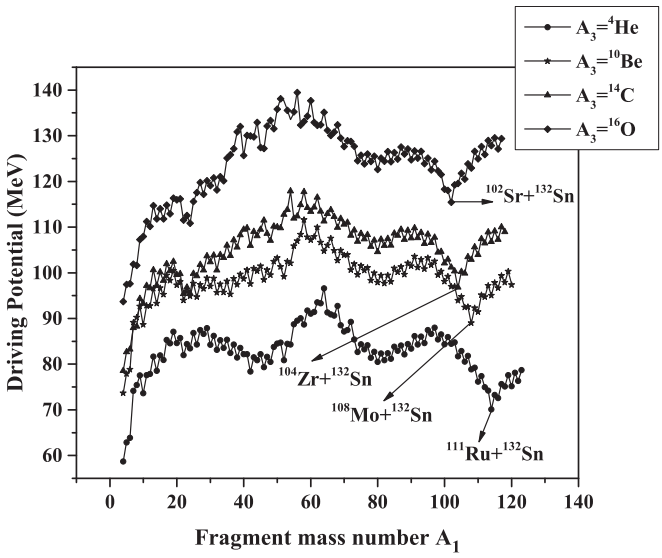

FIG. 1. Driving potential versus fragment mass number A_1 for four groups of accompanying light fragments.

the energy Q released in fission is called driving potential. Q values of individual fragmentation are calculated by using the standard mass tabulated in Refs. [45–48] for the mass of parent and fragments. For ternary fission of the ^{250}Cm isotope as a parent nucleus with a fixed light fragment A_3, the driving potential $(V - Q)$ is evaluated for all possible combinations in the collective coordinate of mass (and charge) asymmetry, $\eta_A = \frac{A_1 - A_2}{A_1 + A_2}$ and $\eta_Z = \frac{Z_1 - Z_2}{Z_1 + Z_2}$, at the touching configuration, respectively. The calculated driving potential as a function of fragment mass number A_1 is indicated in Fig. 1. Since the third fixed fragments considered here are light nuclei, the equatorial configuration is preferred over the collinear structure [36]. In the case where the accompanied third fixed fragment is a heavy nucleus, the collinear configuration is preferred over the equatorial configuration in ternary fission. All possible fragment combinations formed in the ternary fission of ^{250}Cm accompanied with ^{4}He, ^{10}Be, ^{14}C, and ^{16}O light charged particles as fixed fragments have been studied. For example, with ^{10}Be as the fixed third fragment A_3, the remaining part is $A = 240$ which splits into two fragments A_1 and A_2. The possible values for A_1 can change from 4 to 120 increasingly, and consequently A_2 changes from 236 to 120, decreasingly. For each mass pair (A_1, A_2) there is a pair of charges that minimize the driving potential. To obtain the minimized potential, it is necessary to sort out all the possible combinations of $A_1 + A_2$ and then calculate the interaction

TABLE I. Q values, driving potentials V, and relative yields of even-mass fragments for the ^{4}He-accompanied ternary fission of the ^{250}Cm isotope in equatorial touching configuration. (Yields less than 10^{-7} are denoted as "0.")

A_1	A_2	Q (MeV)	V (MeV)	Yield (% × 10^{-3})	A_1	A_2	Q (MeV)	V (MeV)	Yield (% × 10^{-3})
^{4}He	^{242}U	9.520	58.688	0	^{66}Cr	^{180}Yb	139.705	90.880	0
^{8}Be	^{238}Th	12.993	75.419	0	^{68}Mn	^{178}Tm	142.985	92.745	0
^{10}Be	^{236}Th	11.703	73.622	0	^{70}Fe	^{176}Er	153.505	87.124	0.0045
^{12}Be	^{234}Th	4.873	77.840	0	^{72}Co	^{174}Ho	156.035	89.248	0.0021
^{14}C	^{232}Ra	27.048	78.524	0	^{74}Ni	^{172}Dy	167.035	82.658	0.5710
^{16}C	^{230}Ra	22.355	80.943	0	^{76}Ni	^{170}Dy	165.835	83.237	0.2830
^{18}C	^{228}Ra	16.703	84.572	0	^{78}Zn	^{168}Gd	176.408	81.382	4.2301
^{20}O	^{226}Rn	38.022	84.633	0	^{80}Zn	^{166}Gd	176.744	80.476	6.2100
^{22}O	^{224}Rn	38.840	81.965	0	^{82}Ge	^{164}Sm	184.080	80.850	14.7102
^{24}O	^{222}Rn	35.691	83.426	0	^{84}Ge	^{162}Sm	183.243	81.168	9.7703
^{26}Ne	^{220}Po	54.823	84.276	0	^{86}Se	^{160}Nd	188.198	82.927	8.0911
^{28}Ne	^{218}Po	50.916	86.606	0	^{88}Se	^{158}Nd	188.509	82.147	11.2912
^{30}Mg	^{216}Pb	71.969	84.236	0	^{90}Se	^{156}Nd	186.835	83.384	4.2100
^{32}Mg	^{214}Pb	71.575	83.152	0	^{92}Kr	^{154}Ce	191.684	84.279	5.4013
^{34}Mg	^{212}Pb	69.789	83.561	0	^{94}Kr	^{152}Ce	190.973	84.603	3.7721
^{36}Si	^{210}Hg	88.325	82.451	0	^{96}Sr	^{150}Ba	193.745	86.593	2.0400
^{38}Si	^{208}Hg	88.005	81.472	0	^{98}Sr	^{148}Ba	194.581	85.421	3.8598
^{40}Si	^{206}Hg	86.080	82.179	0	^{100}Sr	^{146}Ba	195.335	84.361	6.6711
^{42}S	^{204}Pt	106.123	78.361	0.0002	^{102}Zr	^{144}Xe	199.031	84.470	10.1743
^{44}S	^{202}Pt	102.461	80.870	0	^{104}Zr	^{142}Xe	201.525	81.720	50.5500
^{46}Ar	^{200}Os	119.075	79.329	0.0024	^{106}Zr	^{140}Xe	202.462	80.556	93.9722
^{48}Ar	^{198}Os	116.845	80.471	0.0004	^{108}Mo	^{138}Te	207.023	78.849	370.6401
^{50}Ar	^{196}Os	111.765	84.524	0	^{110}Mo	^{136}Te	209.540	76.154	1706.705
^{52}Ca	^{194}W	129.355	80.886	0.0051	^{112}Ru	^{134}Sn	212.626	74.956	4201.904
^{54}Ca	^{192}W	124.995	84.277	0.0001	^{114}Ru	^{132}Sn	217.331	70.122	49206.00
^{56}Ca	^{190}W	118.845	89.512	0	^{116}Ru	^{130}Sn	214.767	72.585	11189.00
^{58}Ti	^{188}Hf	132.555	88.666	0	^{118}Pd	^{128}Cd	213.196	75.098	3968.303
^{60}Ti	^{186}Hf	129.315	91.044	0	^{120}Pd	^{126}Cd	213.102	75.140	3815.902
^{62}V	^{184}Lu	132.455	93.524	0	^{122}Pd	^{124}Cd	211.883	76.335	1909.00
^{64}V	^{182}Lu	128.615	96.575	0					

TABLE II. Q values, driving potentials V, and relative yields of even-mass fragments for the ^{10}Be-accompanied ternary fission of the ^{250}Cm isotope in equatorial touching configuration. (Yields less than 10^{-7} are denoted as "0.")

A_1	A_2	Q (MeV)	V (MeV)	Yield (% $\times 10^{-3}$)	A_1	A_2	Q (MeV)	V (MeV)	Yield (% $\times 10^{-3}$)
^{4}He	^{236}Th	11.703	73.622	0	^{64}Cr	^{176}Er	140.473	104.7044	0
^{6}He	^{234}Th	2.177	78.797	0	^{66}Cr	^{174}Er	136.873	107.5428	0
^{8}Be	^{232}Ra	14.945	90.206	0	^{68}Fe	^{172}Dy	152.223	102.6534	0
^{10}Be	^{230}Ra	13.260	88.624	0	^{70}Fe	^{170}Dy	150.353	103.8155	0
^{12}Be	^{228}Ra	6.363	92.767	0	^{72}Ni	^{168}Gd	162.969	100.6122	0.0004
^{14}C	^{226}Rn	28.616	93.262	0	^{74}Ni	^{166}Gd	163.373	99.5543	0.0009
^{16}C	^{224}Rn	24.244	95.249	0	^{76}Zn	^{164}Sm	170.786	100.5191	0.0049
^{18}C	^{222}Rn	19.089	98.288	0	^{78}Zn	^{162}Sm	172.396	98.3093	0.0356
^{20}O	^{220}Po	41.324	97.306	0	^{80}Zn	^{160}Sm	172.267	97.8784	0.0359
^{22}O	^{218}Po	42.744	93.959	0	^{82}Ge	^{158}Nd	179.858	97.6557	0.4350
^{24}O	^{216}Po	40.099	94.853	0	^{84}Ge	^{156}Nd	179.001	98.0053	0.1980
^{26}Ne	^{214}Pb	60.085	94.700	0	^{86}Se	^{154}Ce	183.236	100.1259	0.1231
^{28}Ne	^{212}Pb	56.640	96.514	0	^{88}Se	^{152}Ce	183.327	99.5802	0.1610
^{30}Mg	^{210}Hg	74.637	97.032	0	^{90}Se	^{150}Ce	181.03	101.4584	0.0148
^{32}Mg	^{208}Hg	74.482	95.662	0	^{92}Kr	^{148}Ba	186.742	101.1140	0.1021
^{34}Mg	^{206}Hg	73.005	95.724	0	^{94}Kr	^{146}Ba	186.671	100.8178	0.1050
^{36}Si	^{204}Pt	90.693	95.273	0	^{96}Sr	^{144}Xe	190.185	101.6743	0.1442
^{38}Si	^{202}Pt	87.245	97.388	0	^{98}Sr	^{142}Xe	192.038	99.5058	1.1301
^{40}S	^{200}Os	102.001	98.658	0	^{100}Sr	^{140}Xe	193.199	98.0628	3.9303
^{42}S	^{198}Os	101.860	97.544	0	^{102}Zr	^{138}Te	197.673	96.9856	27.9904
^{44}S	^{196}Os	97.867	100.362	0	^{104}Zr	^{136}Te	200.539	93.8885	522.9112
^{46}Ar	^{194}W	114.643	98.434	0	^{106}Zr	^{134}Te	201.829	92.3999	1879.532
^{48}Ar	^{192}W	112.473	99.496	0	^{108}Mo	^{132}Sn	207.689	88.9681	82838.23
^{50}Ar	^{190}W	107.683	103.245	0	^{110}Mo	^{130}Sn	205.065	91.4441	7379.230
^{52}Ca	^{188}Hf	125.523	99.113	0	^{112}Ru	^{128}Cd	203.254	94.6993	455.0322
^{54}Ca	^{186}Hf	121.583	102.073	0	^{114}Ru	^{126}Cd	202.862	94.9939	30.3511
^{56}Ca	^{184}Hf	115.783	106.950	0	^{116}Ru	^{124}Cd	201.1537	96.6362	63.5521
^{58}Sc	^{182}Lu	117.143	111.588	0	^{118}Pd	^{122}Pd	200.3879	97.8831	19.9200
^{60}Ti	^{180}Yb	127.313	107.156	0	^{120}Pd	^{120}Pd	200.9434	97.3120	35.2801
^{62}V	^{178}Tm	129.983	109.967	0					

potential between each conjugate pair. Finally, one may choose the minima of potentials as the most favored combination of $A_1 + A_2$.

As stated earlier, the separation distance between all three fragments is considered equal; however, in the actual situation the light charged particle (third fixed fragment) moves faster than the other two fragments. In other words, the distance of the surface separation between the first and second fragment, s_{12}, is much less than s_{13} and s_{23}, the distances between the light fixed fragment and the main fragments. Although it has been shown [29] that the trend does not change considerably overall the variation of yield for the various fragmentation channels when different distances between fragments are taken in to account. This fact implies that the assumption of equal distances between the fragments, i.e., $s_{12} = s_{13} = s_{23}$, is an acceptable approximation. The deformation and orientation degrees of freedom are not considered in this study. To reduce complexity, the spherical approximation is used for the fragment's shape, which reduces the calculation of potential and yield to a one-dimensional problem. The driving potentials for four groups of fixed light fragments are shown and compared together in Fig. 1. This figure indicates that the lightest charged particle, ^{4}He, possesses the lowest barrier compared with the other three groups. This means that, in the ternary fission of ^{250}Cm, the accompanied ^{4}He group is the most favored. Also, by increasing the mass of the fixed third fragments, the corresponding potential increases dramatically, as shown in Fig. 1. These diagrams imply that, according to the potential minimization with respect to the charge and mass asymmetry, the lighter third fixed fragment, the more favored ternary fission appears in the exit channel. The four most favored channels of the ternary fission of ^{250}Cm accompanied by ^{4}He, ^{10}Be, ^{14}C, and ^{16}O as fixed light fragments are ^{132}Sn + ^{111}Ru + ^{4}He, ^{132}Sn + ^{108}Mo + ^{10}Be, ^{132}Sn + ^{104}Zr + ^{14}C, and ^{132}Sn + ^{102}Sr + ^{16}O, in order from the most to the least favorite. As is obvious, all these favored fragmentation channels include the doubly-closed-shell nucleus, ^{132}Sn ($Z = 50$, $N = 82$). Using Eq. (9), the relative yields of each combinations of fragments for the ^{16}O-accompanied light fragment are calculated and indicated in Fig. 6 as a function of fragment mass number A_1. As is clear from this figure, the odd-mass fragments have smaller relative yields compared with the even-mass neighbor fragments. The obtained Q values and driving potentials $V - Q$ for various ternary fragmentations are shown in Tables I–IV. Generally, since the odd-mass fragments are less favored than the even-mass fragments, only even-mass-

TABLE III. Q values, driving potentials V, and relative yields of even-mass fragments for the ^{14}C-accompanied ternary fission of the ^{250}Cm isotope in equatorial touching configuration. (Yields less than 10^{-7} are denoted as "0.")

A_1	A_2	Q (MeV)	V (MeV)	Yield (% × 10^{-3})	A_1	A_2	Q (MeV)	V (MeV)	Yield (% × 10^{-3})
^{4}He	^{232}Ra	27.0480	78.5237	0	^{62}V	^{174}Ho	141.1401	116.4803	0
^{6}He	^{230}Ra	17.8620	83.2564	0	^{64}Cr	^{172}Dy	151.4401	111.252	0
^{8}He	^{228}Ra	9.4180	88.2354	0	^{66}Cr	^{170}Dy	148.1701	113.7693	0
^{10}Be	^{226}Rn	28.6160	93.2627	0	^{68}Fe	^{168}Gd	162.1601	109.9096	0
^{12}Be	^{224}Rn	22.4470	96.623	0	^{70}Fe	^{166}Gd	160.8101	110.5611	0
^{14}C	^{222}Po	44.4601	97.2426	0	^{72}Ni	^{164}Sm	172.2961	108.1429	0.0002
^{16}C	^{220}Po	41.0131	98.2603	0	^{74}Ni	^{162}Sm	172.9601	106.8348	0.0005
^{18}C	^{218}Po	36.6913	100.4338	0	^{76}Ni	^{160}Sm	171.8151	107.3799	0.0001
^{20}O	^{216}Pb	58.6939	99.5355	0	^{78}Zn	^{158}Nd	181.5133	105.7104	0.0251
^{22}O	^{214}Pb	60.8709	95.404	0	^{80}Zn	^{156}Nd	182.0887	104.5878	0.0588
^{24}O	^{212}Pb	59.0173	95.4862	0	^{82}Ge	^{154}Ce	187.7352	105.9337	0.1271
^{26}Ne	^{210}Hg	74.8611	99.2978	0	^{84}Ge	^{152}Ce	187.1781	105.9964	0.0712
^{28}Ne	^{208}Hg	71.9501	100.5605	0	^{86}Ge	^{150}Ce	184.5771	108.1427	0.0031
^{30}Mg	^{206}Pt	88.4841	102.3412	0	^{88}Se	^{148}Ba	191.4441	107.2543	0.0731
^{32}Mg	^{204}Pt	88.7191	100.5661	0	^{90}Se	^{146}Ba	190.7101	107.5853	0.0330
^{34}Si	^{202}Os	103.0171	103.2998	0	^{92}Kr	^{144}Xe	195.6111	107.645	0.1592
^{36}Si	^{200}Os	101.1401	103.7345	0	^{94}Kr	^{142}Xe	196.5477	106.3572	0.5468
^{38}Si	^{198}Os	97.9801	105.5535	0	^{96}Kr	^{140}Xe	196.0366	106.5537	0.3168
^{40}Si	^{196}Os	92.8201	109.4648	0	^{98}Sr	^{138}Te	202.0921	104.4625	012.42
^{42}S	^{194}W	112.1381	105.9189	0	^{100}Sr	^{136}Te	204.2259	102.0652	157.47
^{44}S	^{192}W	108.8241	108.0543	0	^{102}Sr	^{134}Te	204.8661	101.1969	344.72
^{46}Cl	^{190}Ta	112.2901	111.4642	0	^{104}Zr	^{132}Sn	212.244	96.7932	92595
^{48}Ar	^{188}Hf	123.2901	107.0646	0	^{106}Zr	^{130}Sn	209.013	99.8467	3005.7
^{50}Ar	^{186}Hf	119.3101	110.0048	0	^{108}Mo	^{128}Cd	207.9741	102.858	187.59
^{52}K	^{184}Lu	122.9201	112.7541	0	^{110}Mo	^{126}Cd	206.7759	103.9294	49.76
^{54}K	^{182}Lu	116.8501	117.8783	0	^{112}Mo	^{124}Cd	204.1318	106.4808	2.48
^{56}Ca	^{180}Yb	128.4701	112.3772	0	^{114}Ru	^{122}Pd	204.8081	106.7942	2.33
^{58}Sc	^{178}Tm	128.9701	117.7304	0	^{116}Ru	^{120}Pd	204.3193	107.2408	1.39
^{60}Ti	^{176}Er	138.9301	113.3606	0	^{118}Ru	^{118}Pd	202.619	108.9328	0.1872

fragment combinations are presented in these tables. As it turns out from the data of these tables, the relative yield of ternary fission is dramatically increased upon decreasing the mass difference between fragments A_1 and A_2. In the following, the fragmentation with ^{4}He, ^{10}Be, ^{14}C, and ^{16}O as fixed third fragments are analyzed separately in different subsections.

A. ^{4}He-accompanied ternary fission of ^{250}Cm

From Fig. 2, it is clear that the combination ^{114}Ru + ^{132}Sn + ^{4}He possess the highest yield due to the presence of the doubly magic nucleus ^{132}Sn ($Z = 50$, $N = 82$). The next-higher yield can be seen for the combination ^{116}Ru + ^{130}Sn + ^{4}He that is due to the even-even magic ^{130}Sn ($Z = 50$, $N = 80$) nucleus. By comparing the graphs of Figs. 1 and 2, it is easily understood that each cold reaction valley in the driving potential diagram is equivalent to a peak in the relative yield diagram. The other various peaks in the relative yield graph of Fig. 2 correspond to fragment combinations ^{82}Ge + ^{164}Sm + ^{4}He, ^{110}Mo + ^{136}Te + ^{4}He, ^{118}Pd + ^{128}Cd + ^{4}He, and ^{120}Pd + ^{126}Cd + ^{4}He. Among these combinations, the first one is attributed to the magic neutron shell $N = 50$ of ^{82}Ge, and the second combination is due to the near doubly closed shell ($Z = 52$, $N = 84$) of ^{136}Te nucleus. The fragment combination with ^{128}Cd isotope is also favored due to the presence of an even-even, nearly closed shell ($Z = 48$, $N = 80$).

B. ^{10}Be-accompanied ternary fission of ^{250}Cm

With ^{10}Be as the fixed third fragment, the deepest minimum in the cold reaction valley of driving potential belongs to ^{108}Mo + ^{132}Sn + ^{10}Be fragmentation (Fig. 1). Therefore, the highest maximum of the yield graph is belongs to the fragment combination ^{108}Mo + ^{132}Sn + ^{10}Be (Fig. 3). As mentioned earlier, this favorable channel is due to presence of the doubly magic closed-shell nucleus ^{132}Sn ($Z = 50$, $N = 82$). The next peak of the relative yield graph in Fig. 3 comes from the fragment combination of ^{110}Mo + ^{130}Sn + ^{10}Be, similarly due to the magic proton number ($Z = 50$) and nearly magic even neutron number ($N = 80$). The other notable peaks are also shown in the Fig. 3.

C. ^{14}C-accompanied ternary fission of ^{250}Cm

In the case of ^{14}C as the fixed third fragment, the highest maximum of the yield belongs to the fragment combination ^{104}Zr + ^{132}Sn + ^{14}C, which happens just like the two previous cases due to the double magic number of protons and neutrons

TABLE IV. Q values, driving potentials V, and relative yields of even-mass fragments for the ^{16}O-accompanied ternary fission of the ^{250}Cm isotope in equatorial touching configuration. (Yields less than 10^{-7} are denoted as "0.")

A_1	A_2	Q (MeV)	V (MeV)	Yield (% × 10^{-3})	A_1	A_2	Q (MeV)	V (MeV)	Yield (% × 10^{-3})
^{4}He	^{230}Rn	33.252	93.7180	0	^{64}V	^{170}Tb	140.617	135.1354	0
^{6}He	^{228}Rn	24.892	97.5882	0	^{66}Cr	^{168}Gd	150.627	130.0538	0
^{8}He	^{226}Rn	17.3703	101.6274	0	^{68}Mn	^{166}Eu	152.957	132.3927	0
^{10}Be	^{224}Po	35.2095	107.9348	0	^{70}Fe	^{164}Sm	162.137	127.6241	0
^{12}Be	^{222}Po	30.159	110.1594	0	^{72}Fe	^{162}Sm	160.357	128.7597	0
^{14}C	^{220}Pb	51.037	111.7901	0	^{74}Ni	^{160}Nd	173.317	124.5016	0.0004
^{16}C	^{218}Pb	48.583	111.7979	0	^{76}Ni	^{158}Nd	173.397	123.8287	0.0005
^{18}C	^{216}Pb	45.327	112.8966	0	^{78}Ni	^{156}Nd	172.327	124.3506	0.0001
^{20}C	^{214}Pb	40.3478	115.9554	0	^{80}Zn	^{154}Ce	181.7256	122.600	0.0510
^{22}O	^{212}Hg	65.687	111.5111	0	^{82}Zn	^{152}Ce	179.397	124.4306	0.0019
^{24}O	^{210}Hg	64.597	110.8260	0	^{84}Ge	^{150}Ba	186.125	124.3026	0.0451
^{26}O	^{208}Hg	56.267	117.5437	0	^{86}Ge	^{148}Ba	185.077	124.9032	0.0110
^{28}Ne	^{206}Pt	76.067	117.1595	0	^{88}Se	^{146}Xe	189.566	125.9752	0.0265
^{30}Ne	^{204}Pt	72.607	119.1046	0	^{90}Se	^{144}Xe	190.399	124.7454	0.0914
^{32}Mg	^{202}Os	91.646	118.1279	0	^{92}Se	^{142}Xe	189.6766	125.1107	0.0363
^{34}Mg	^{200}Os	88.184	120.1642	0	^{94}Kr	^{140}Te	195.432	123.8961	1.1900
^{36}Mg	^{198}Os	81.187	125.8429	0	^{96}Kr	^{138}Te	196.503	122.5178	5.3000
^{38}Al	^{196}Re	84.057	130.8699	0	^{98}Kr	^{136}Te	196.4628	122.2887	5.2900
^{40}Si	^{194}W	96.827	125.6990	0	^{100}Sr	^{134}Sn	203.989	118.291	3257.10
^{42}P	^{192}Ta	99.877	129.9554	0	^{102}Sr	^{132}Sn	206.6309	115.4291	89535.00
^{44}P	^{190}Ta	95.797	132.9073	0	^{104}Zr	^{130}Cd	204.987	119.5824	1290.900
^{46}S	^{188}Hf	108.567	127.1865	0	^{106}Zr	^{128}Cd	203.879	120.5199	324.490
^{48}S	^{186}Hf	101.387	133.3434	0	^{108}Zr	^{126}Cd	201.3338	122.9309	12.750
^{50}Cl	^{184}Lu	105.707	135.8164	0	^{110}Mo	^{124}Pd	200.826	124.9454	1.6600
^{56}K	^{178}Tm	113.917	139.4794	0	^{112}Mo	^{122}Pd	199.803	125.8834	0.4331
^{58}Ca	^{176}Er	126.277	133.1099	0	^{114}Mo	^{120}Pd	197.8172	127.8202	0.0311
^{60}Sc	^{174}Ho	127.467	137.6409	0	^{116}Ru	^{118}Ru	199.056	127.0878	0.1045
^{62}Ti	^{172}Dy	138.307	132.2552	0					

in ^{132}Sn ($Z = 50$, $N = 82$). The other remarkable peaks are also indicated in Fig. 4.

D. ^{16}O-accompanied ternary fission of ^{250}Cm

For ternary fission of ^{250}Cm with ^{16}O as the fixed third fragment, the deepest minimum in the cold reaction valley

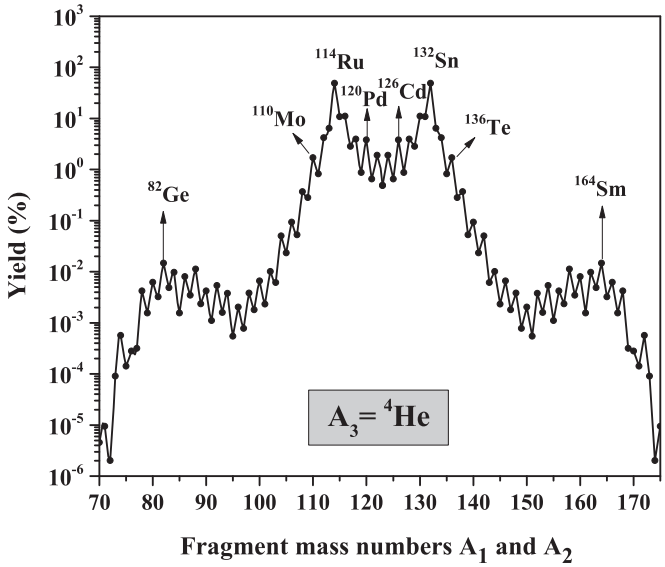

FIG. 2. Relative yield for ^{4}He-accompanied ternary fission of ^{250}Cm as a function of mass numbers A_1 and A_2.

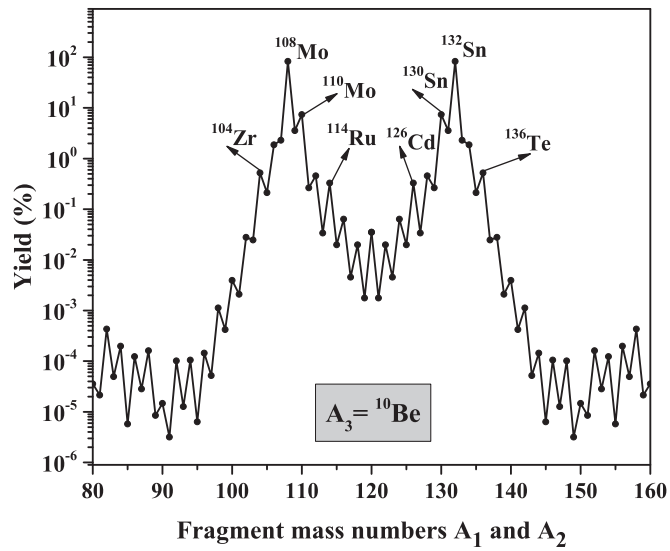

FIG. 3. Relative yield for ^{10}Be-accompanied ternary fission of ^{250}Cm as a function of mass numbers A_1 and A_2.

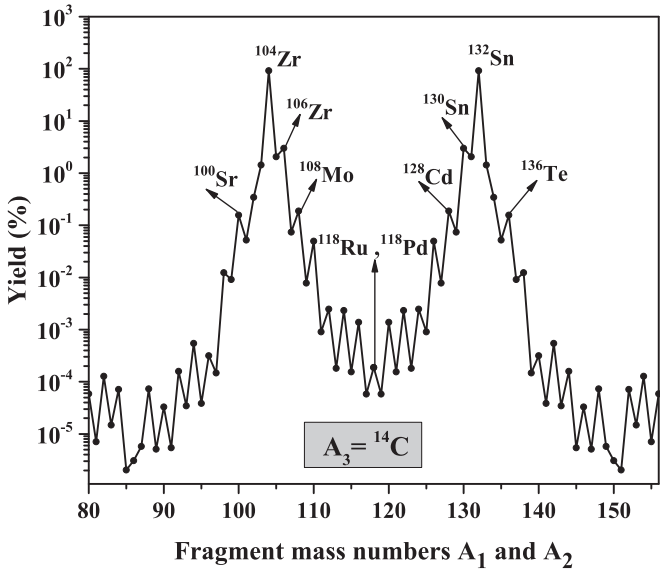

FIG. 4. Relative yield for ^{14}C-accompanied ternary fission of ^{250}Cm as a function of mass numbers A_1 and A_2.

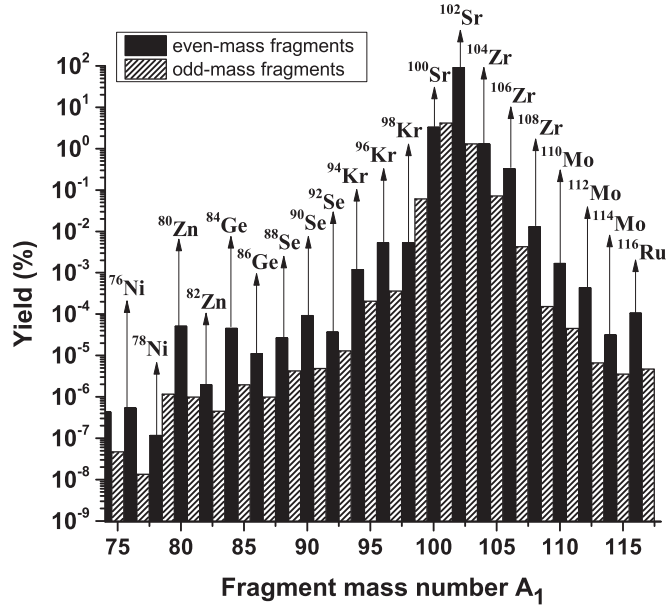

FIG. 6. Relative yield for ^{16}O-accompanied ternary fission of ^{250}Cm as a bar graph.

of the driving potential belongs to the ^{102}Sr + ^{132}Sn + ^{16}O fragmentation (Fig. 1). As is evident from Fig. 5, the highest maximum of the yield graph belongs to this combination. The next maximum in the relative yield graph for ^{16}O-accompanied ternary fission of ^{250}Cm comes from the fragment combination of ^{100}Sr + ^{134}Sn + ^{16}O, which is likewise due to the presence of the magic proton number ($Z = 50$) and nearly magic even neutron number ($N = 84$) of ^{134}Sn nucleus. The other distinguished peaks of yield are also shown in Figs. 5 and 6.

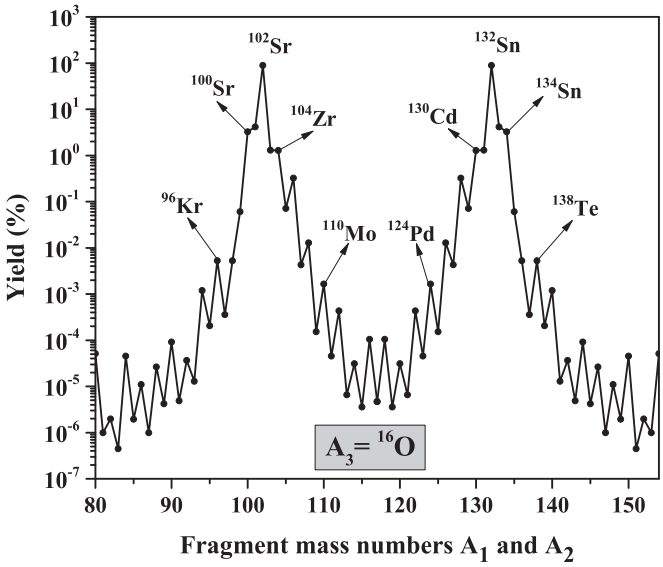

FIG. 5. Relative yield for ^{16}O-accompanied ternary fission of ^{250}Cm as a function of mass numbers A_1 and A_2.

IV. CONCLUSION

The cold ternary fission of ^{250}Cm accompanied by ^{4}He, ^{10}Be, ^{14}C, and ^{16}O as the fixed light fragments in the equatorial geometry configuration have been studied by using the three-cluster model [38]. In each case, the driving potentials, Q values, and relative yields are calculated for all possible fragmentations. The results of the calculation indicate that the components with even mass numbers are more favored than the components with odd mass numbers. From the results, it can be concluded that, upon increasing the mass of the third fixed fragment in ternary fission, the probability of crossing over the potential barrier is considerably decreased due to growth in the height of potential barrier. Thus, the lighter third fixed fragment is more probable in ternary fragmentation. Comparison between relative yields for a variety of fragmentation in each group (with ^{4}He, ^{10}Be, ^{14}C, and ^{16}O as the fixed third fragment) reveals that the presence of a doubly magic closed shell or near-doubly-magic nuclei plays an important role in the cold ternary fission of ^{250}Cm. In the first group with ^{4}He as the third fragment, the maximum yield is obtained for the combination ^{114}Ru + ^{4}He + ^{132}Sn due to the presence of doubly magic nucleus ^{132}Sn ($N = 82$, $Z = 50$). Similarly, for the three other groups (^{10}Be, ^{14}C, and ^{16}O as third fragment), fragmentations ^{108}Mo + ^{10}Be + ^{132}Sn, ^{104}Zr + ^{14}C + ^{132}Sn, and ^{102}Sr + ^{16}O + ^{132}Sn are produced as the most favorable combinations, respectively. In addition, it can be found from Tables I–IV that, for a certain fixed fragment, the binary combinations with little mass difference are preferred, generally. This theoretical work can be developed to consider heavier third fixed fragments and for different parent nuclei to compare equatorial and collinear geometry of fragmentation.

[1] Tsien San-Tsiang, Ho Zah-Wei, R. Chastel, and L. Vigneron, J. Phys. Radium **8**, 165 (1947).
[2] Tsien San-Tsiang, Ho Zah-Wei, L. Vigneron, and R. Chastel, Nature (London) **159**, 773 (1947).
[3] D. N. Poenaru, M. Ivascu, and M. S. Ivaşcu, in *Particle Emission from Nuclei* (CRC Press, Boca Raton, Florida, 1989), Vol. 3, Chap. 3, pp. 63–97.
[4] D. N. Poenaru, in *Nuclear Decay Modes* (Institute of Physics Publishing, Bristol, UK, 1996), Vol. 27, Issue 17, Chap. 12.
[5] D. N. Poenaru *et al.*, in *Clusters in Nuclei* (Springer, Berline, 2010), Vol. 1, Chap. 1, pp. 1–56.
[6] O. Serot *et al.*, Proc. Int. Conf. Nuclear Data for Science and Technology (2007), doi:10.1051/ndata:07748.
[7] E. L. Albenesius, Phys. Rev. Lett. **3**, 274 (1959).
[8] E. L. Albenesius and R. S. Ondrejcin, Nucleonics **18**, 100 (1960).
[9] W. von Oertzen and A. K. Nasirov, Phys. Lett. B **734**, 234 (2014).
[10] L. W. Alvarez, G. Farwell, E. Segrè, and C. Wiegand, Phys. Rev. **71**, 327 (1947).
[11] L. L. Green and D. L. Livesey, Nature (London) **159**, 332 (1947).
[12] T. P. Doan, C. Carles, and R. Chastel, Nucl. Phys. A **96**, 588 (1967).
[13] P. Fong, Phys. Rev. C **2**, 735 (1970).
[14] P. B. Vitta, Nucl. Phys. A **170**, 417 (1971).
[15] C. Wagemans and A. J. Deruytter, Nucl. Phys. A **194**, 657 (1972).
[16] J. P. Theobald, P. Heeg, and M. Mutterer, Nucl. Phys. A **502**, 343 (1989).
[17] G. Royer, F. Haddad, and J. Mignen, J. Phys. G **18**, 2015 (1992).
[18] A. Sándulescu, F. Carstoiu, I. Bulboaca, and W. Greiner, Phys. Rev. C **60**, 044613 (1999).
[19] D. N. Poenaru, W. Greiner, J. H. Hamilton, A. V. Ramayya, E. Hourany, and R. A. Gherghescu, Phys. Rev. C **59**, 3457 (1999).
[20] A. Florescu, A. Sándulescu, D. S. Delion, J. H. Hamilton, A. V. Ramayya, and W. Greiner, Phys. Rev. C **61**, 051602(R) (2000).
[21] F. Carstoiu, I. Bulboaca, A. Sándulescu, and W. Greiner, Phys. Rev. C **61**, 044606 (2000).
[22] S. Misicu, P. O. Hess, and W. Greiner, Phys. Rev. C **63**, 054308 (2001).
[23] D. S. Delion, A. Florescu, and A. Sándulescu, Phys. Rev. C **63**, 044312 (2001).
[24] L. Rosen and A. M. Hudson, Phys. Rev. **78**, 533 (1950).
[25] D. N. Poenaru, B. Dobrescu, W. Greiner, J. H. Hamilton, and A. V. Ramayya, J. Phys. G **26**, L97 (2000).
[26] D. N. Poenaru, R. A. Gherghescu, W. Greiner, Y. Nagame, J. H. Hamilton, and A. V. Ramayya, Rom. Rep. Phys. **55**, 549 (2003).
[27] D. N. Poenaru, R. A. Gherghescu, and W. Greiner, Nucl. Phys. A **747**, 182 (2005).
[28] K. Manimaran and M. Balasubramaniam, Eur. Phys. J. A **45**, 293 (2010).
[29] K. Manimaran and M. Balasubramaniam, Phys. Rev. C **83**, 034609 (2011).
[30] S. S. Malik and R. K. Gupta, Phys. Rev. C **39**, 1992 (1989).
[31] R. K. Gupta, W. Scheid, and W. Greiner, J. Phys. G **17**, 1731 (1991).
[32] S. Kumar and R. K. Gupta, Phys. Rev. C **49**, 1922 (1994).
[33] K. Manimaran and M. Balasubramaniam, J. Phys. G **37**, 045104 (2010).
[34] K. R. Vijayaraghavan, W. von Oertzen, and M. Balasubramaniam, Eur. Phys. J. A **48**, 27 (2012).
[35] K. R. Vijayaraghavan, Ph.D. thesis, Bharathiar University, 2015 (unpublished).
[36] K. R. Vijayaraghavan, M. Balasubramaniam, and W. von Oertzen, Phys. Rev. C **90**, 024601 (2014).
[37] M. Balasubramaniam, K. R. Vijayaraghavan, and K. Manimaran, Phys. Rev. C **93**, 014601 (2016).
[38] K. P. Santhosh, S. Krishnan, and B. Priyanka, Eur. Phys. J. A **50**, 66 (2014).
[39] K. P. Santhosh, S. Krishnan, and B. Priyanka, Int. J. Mod. Phys. E **23**, 1450071 (2014).
[40] V. Mirzaei and H. Miri-Hakimabad, Rom. Rep. Phys. **64**, 50 (2012).
[41] Yu. N. Kopatch, M. Mutterer, D. Schwalm, P. Thirolf, and F. Gonnenwein, Phys. Rev. C **65**, 044614 (2002).
[42] J. H. Hamilton *et al.*, Phys. At. Nucl. **65**, 645 (2002).
[43] K. P. Santhosh and S. Krishnan, Eur. Phys. J. A **52**, 108 (2016).
[44] J. Blocki and W. J. Swiatecki, Ann. Phys. (NY) **132**, 53 (1983).
[45] G. Audi and A. H. Wapstra, Nucl. Phys. A **595**, 409 (1995).
[46] A. H. Wapstra, G. Audi, and C. Thibault, Nucl. Phys. A **729**, 129 (2003).
[47] G. Audi *et al.*, Chin. Phys. C **36**, 1603 (2012).
[48] D. N. Poenaru, W. Greiner, and R. A. Gherghescu, At. Data Nucl. Data Tables **68**, 91 (1998).